Moving doubly heavy baryon in a strongly coupled plasma via holography*

Xuan Liu (刘旋)[1] Jia-Jie Jiang (江佳杰)[1] Xun Chen (陈勋)[1†] Mitsutoshi Fujita[1‡] Akira Watanabe[2§]

[1]School of Nuclear Science and Technology, University of South China, Hengyang 421001, China
[2]School of Mathematics and Physics, University of South China, Hengyang 421001, China

Abstract: Gauge/gravity duality is used to study the properties of the doubly heavy baryon (QQq) at finite rapidity and temperature in heavy-ion collisions. We investigate the impact of rapidity on string breaking and screening of QQq and compare these effects with the results for $Q\bar{Q}$ in detail. Computations reveal that the string-breaking distances of QQq and $Q\bar{Q}$ are close in the confined state, and the effects of rapidity and temperature on the string breaking are not significant. An interesting result shows that QQq cannot be determined at sufficiently high temperatures and rapidities. However, $Q\bar{Q}$ can exist under any conditions as long as the separation distance is sufficiently small. Furthermore, the screening distances of QQq and $Q\bar{Q}$ are compared at finite rapidity and temperature. Based on the above analysis, we infer that $Q\bar{Q}$ is more stable than QQq at finite rapidity and temperature.

Keywords: holographic QCD, QGP, heavy quark

DOI: 10.1088/1674-1137/ad39cf

I. INTRODUCTION

In the recent LHCb experiment at CERN, researchers reported an exciting discovery of a particle known as Ξ_{cc}^{++} [1, 2]. This groundbreaking finding has sparked significant interest in the exploration of double charm baryons. Specifically, the Ξ_{cc}^{++} particle is formed by the combination of two heavy quarks with a single light quark, resulting in a highly distinctive structure. In this study, we adopt an assumption of potential models, which suggests that the interaction between heavy quarks and anti-quarks within hadrons can be described by a potential energy [3].

Although lattice gauge theory remains a fundamental tool for studying non-perturbative phenomena in Quantum Chromodynamics (QCD), its investigation of the doubly heavy baryon potential has been relatively limited to date [4, 5]. In contrast, gauge/gravity duality provides a new theoretical tool for studying strongly coupled gauge theories. Furthermore, in Ref. [6], the holographic potential of quark-antiquark pairs was computed for the first time. Based on the study in Ref. [6], the potential was further investigated in Refs. [7, 8] to examine the potential at finite temperature. In recent years, the methodology of utilizing holographic theories to study multi-quark potentials has been increasingly refined. The obtained multi-quark potentials from holography are in good agreement with lattice calculations and QCD phenomenology [9–20]. The techniques employed to extract the QQq potential in our study are analogous to those used in lattice QCD [21].

The creation of quark-gluon plasma (QGP) via high-energy heavy-ion collisions allows us to simulate the high temperature and density conditions of the early universe [22–25]. The formation of this QGP is crucial for our understanding of the early stages of cosmic evolution and the fundamental properties of quark color dynamics. At low temperatures, quarks and gluons are confined within hadrons. As the separation between quarks increases, the strong interaction force becomes stronger. When the separation reaches a limit, new quark-antiquark pairs are typically produced, resulting in the confinement of quarks within hadrons. This behavior is manifested as string breaking in this study. Under extreme conditions, the strong interaction between hadrons diminishes at long range, allowing quarks to move freely over larger distances [26–28].

In heavy-ion collision experiments, heavy ions collide at speeds close to the speed of light, forming QGP

Received 29 January 2024; Accepted 3 April 2024; Published online 4 April 2024

* Supported by the Natural Science Foundation of Hunan Province, China (2022JJ40344), and the Research Foundation of Education Bureau of Hunan Province, China (21B0402)

† E-mail: chenxunhep@qq.com
‡ E-mail: fujitamitsutoshi@usc.edu.cn
§ E-mail: watanabe@usc.edu.cn

[25]. Similar to the early universe, this substance does not remain stationary but rapidly expands. Therefore, when studying the doubly heavy baryon, the effect of rapidity should be considered. This is crucial for understanding the interaction between QQq and the medium, as well as the transport properties within the QGP. By examining the behavior of moving QQq, more comprehensive information about the QGP can be obtained, leading to further investigation into the properties of QCD. Furthermore, by studying the variation in string breaking under different temperature and rapidity conditions, we can investigate decay rates of different hadrons under varying conditions [29].

Gauge/gravity duality was initially proposed by Maldacena [30] for conformal field theories, and it was later extended to include theories resembling QCD, establishing a connection between string theory and heavy-ion collisions in some manner [31−33]. The study of moving heavy quarkonium can be found in Refs. [34−50].

The remaining sections of this paper are as follows. In Sec. II, we construct string configurations considering the effects of finite temperature and finite rapidity. In Sec. III, we discuss the computation of the model's potential energy. At first, we calculate the influence of rapidity on the string breaking of QQq. Then, we discuss its screening and provide a comprehensive comparison with $Q\bar{Q}$. Additionally, we plot their state diagrams in the $T-\eta$ plane. Finally, we summarize these findings in Sec. IV.

II. MODEL SETUP

First, the background metric at a finite temperature can be expressed as [13, 14, 51−53]:

$$\mathrm{d}s^2 = w(r)\left(-f(r)\mathrm{d}t^2 + \mathrm{d}\vec{x}^2 + \frac{1}{f(r)}\mathrm{d}r^2\right) + \mathrm{e}^{-\mathbf{s}r^2} g^{(5)}_{ab}\mathrm{d}\omega^a \mathrm{d}\omega^b, \quad (1)$$

where

$$w(r) = \frac{\mathrm{e}^{\mathbf{s}r^2}R^2}{r^2},$$
$$f(r) = 1 - \frac{r^4}{r_h^4}. \quad (2)$$

The metric represents a one-parameter deformation of Euclidean $\mathrm{AdS}_5 \times \mathrm{S}_5$ space, parametrized by $\mathbf{s}$ and with a radius R. It comprises a five-dimensional compact space (sphere) X with coordinates ω^a, a blackening factor $f(r)$, and a black hole horizon (brane) at r_h. The Hawking temperature of the black hole T is defined as follows:

$$T = \frac{1}{4\pi}\left|\frac{\mathrm{d}f}{\mathrm{d}r}\right|_{r=r_h} = \frac{1}{\pi r_h}. \quad (3)$$

In this study, we investigate the motion of a particle comprising two heavy quarks and one light quark in a thermal medium. We divide the particle's spatial coordinates into three directions: x_1 (connecting the heavy quark pair), x_2, and x_3 (perpendicular to the heavy quark pair). We determine that the coefficients of x_1 and x_2 in the metric are the same, which implies that the presence of the heavy quark pair at either x_1 or x_2 does not affect the calculation results. Given that temperature and rapidity are constant, we can consider the doubly heavy baryon to be in a state of force equilibrium. Furthermore, energy loss is not considered in this study. Hence, it can be discussed in future studies.

In our study, we consider that QQq is moving with a constant rapidity η along x_3 direction [34−36, 43, 46]. For convenience, let us consider a new scenario in which QQq is at rest, while the surrounding medium is in motion relative to it. We then introduce the Lorentz transform to reflect the effect of rapidity η on it and obtain the new metric:

$$\mathrm{d}s^2 = w(r)\Big(-g_1(r)\mathrm{d}t^2 - 2\sinh(\eta)\cosh(\eta)\Big(1-\frac{g_1(r)}{g_2(r)}\Big)\mathrm{d}x_3\mathrm{d}t + g_3(r)\mathrm{d}x_3^2 + \mathrm{d}x_1^2 + \mathrm{d}x_2^2 + \frac{g_2(r)}{g_1(r)}\mathrm{d}r^2\Big) + \mathrm{e}^{-\mathbf{s}r^2} g^{(5)}_{ab}\mathrm{d}\omega^a\mathrm{d}\omega^b, \quad (4)$$

where

$$g_1(r) = f(r)\cosh^2(\eta) - \sinh^2(\eta),$$
$$g_2(r) = \frac{g_1(r)}{f(r)},$$
$$g_3(r) = \cosh^2(\eta) - f(r)\sinh^2(\eta). \quad (5)$$

The Nambu-Goto action of a string can be expressed as follows:

$$S_{NG} = -\frac{1}{2\pi\alpha'}\int \mathrm{d}\xi^0\mathrm{d}\xi^1\sqrt{-\det g_{ab}}, \quad (6)$$

where α' denotes a constant, (ξ^0, ξ^1) denote worldsheet coordinates, and g_{ab} denotes an induced metric. We introduce the baryon vertex and heavy and light quarks to construct the QQq configuration. Then, we know from AdS/CFT that the vertex is a five brane [54, 55]. At leading order in α', the baryon vertex action is $S_{\mathrm{vert}} = \tau_5\int \mathrm{d}^6\xi\sqrt{\gamma^{(6)}}$, where τ_5 denotes the brane tension and ξ^i denotes the worldvolume coordinates. Given that the brane is wrapped on X interior space, it looks point-like in AdS_5. We select a static gauge $\xi^0 = t, \xi^a = \theta^a$ with θ^a as the coordinates on X. Hence, the following holds.

$$S_{\mathrm{vert}} = \tau_v\int \mathrm{d}t\frac{\mathrm{e}^{-2\mathbf{s}r^2}}{r}\sqrt{g_1(r)}, \quad (7)$$

where τ_v denotes a dimensionless parameter defined by $\tau_v = \tau_5 R\mathrm{vol(X)}$ and vol(X) denotes a volume of X.

Finally, we consider the light quark at the end of the string as a tachyon field, which couples to the worldsheet boundary by $S_q = \int \mathrm{d}\tau \mathbf{e} T$ [56, 57]. This term is typical for strings propagating in an open string tachyon background and T is its background scalar [56]. The integral over a worldsheet boundary, parameterized by τ and $\mathbf{e}$, represents the boundary metric. In this study, we can assume T to be a constant T_0, and the integral reduces to a coordinate integral of t. Thus, the the following holds.

$$S_q = m\int \mathrm{d}t \frac{\mathrm{e}^{\frac{\mathbf{s}r^2}{2}}}{r}\sqrt{g_1(r)}, \tag{8}$$

where $m = RT_0$. This shows that a particle with mass T_0 is at rest, while the surrounding medium with temperature T moves relative to it with rapidity η. The selected parameters are as follows: $g = \dfrac{R^2}{2\pi\alpha'} = 0.176$, $k = \dfrac{\tau_v}{3g} = -0.321$, $n = \dfrac{m}{g} = 3.057$, $\mathbf{s} = 0.45\,\mathrm{GeV}^2$, $c = 0.623\,\mathrm{GeV}$ [20].

A. Small L

As shown in Fig. 1, the heavy quark pair, light quark, and baryon vertex are connected by three strings. Specifically, the separation distance between the heavy quark pair is denoted as L. Therefore, we can express the total action as follows:

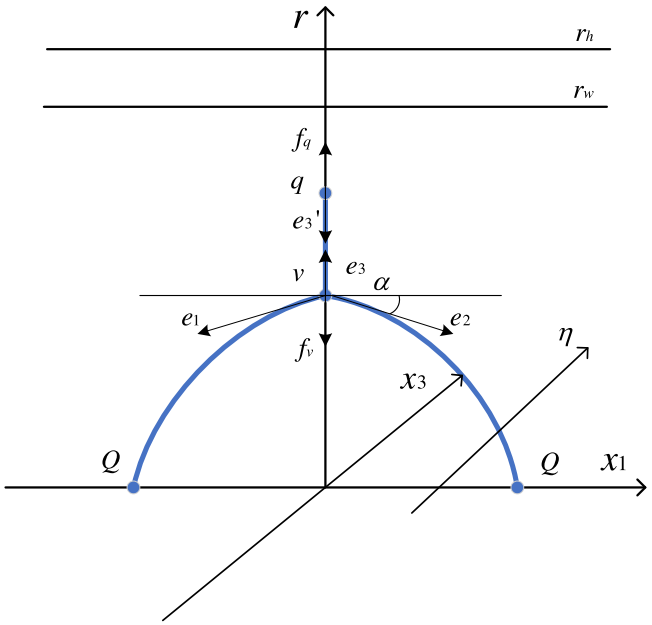

Fig. 1. (color online) String configuration at a small separation distance of heavy quark pair. We use the line connecting two heavy quarks Q as the x_1-axis, while the baryon vertex v and light quark q are on the r-axis. The rapidity η is along the x_3-axis direction. The heavy quark, light quark, and baryon vertex are connected by blue strings. The black arrows represent generalized forces. Furthermore, r_h denotes the position of the black hole horizon. r_w denotes the position of an imaginary wall when QQq is confined.

$$S = \sum_{i=1}^{3} S_{\mathrm{NG}}^{(i)} + S_{\mathrm{vert}} + S_q. \tag{9}$$

According to a previous discussion, given that the results obtained from x_1 and x_2 are the same, we directly designate the line where the heavy quark pair is located as x_1. Furthermore, the rapidity perpendicular to the x_1 direction corresponds to x_3, as shown in Fig. 1. Hereafter, we refer to x_1 as x. Then, in this configuration, we choose the static gauge where $\xi^0 = t$, $\xi^1 = r$, and we consider x as a function of r. Therefore, the total sum of the Nambu-Goto action can be expressed as:

$$\begin{aligned}\sum_{i=1}^{3} S_{\mathrm{NG}}^{(i)} = {} & 2g\int_0^t \mathrm{d}t\int_0^{r_v} w(r)\sqrt{g_1(r)(\partial_r x)^2 + g_2(r)}\mathrm{d}r \\ & + g\int_0^t \mathrm{d}t\int_{r_v}^{r_q} w(r)\sqrt{g_1(r)(\partial_r x)^2 + g_2(r)}\mathrm{d}r,\end{aligned} \tag{10}$$

where $\partial_r x = \dfrac{\partial x}{\partial r}$ and $x(r)$ satisfy the following boundary conditions:

$$\begin{aligned} & x(0) = \pm\frac{L}{2},\ x(r_v) = x(r_q) = 0, \\ & \begin{cases} (\partial_r x)^2 = \cot^2(\alpha), & r = r_v \\ (\partial_r x)^2 = 0, & r \in (r_v, r_q]. \end{cases}\end{aligned} \tag{11}$$

Now, we combine the baryon vertex and light quark as follows:

$$\begin{aligned} S = gt\Big(2\int_0^{r_v} & w(r)\sqrt{g_1(r)(\partial_r x)^2 + g_2(r)}\mathrm{d}r \\ & + \int_{r_v}^{r_q} w(r)\sqrt{g_2(r)}\mathrm{d}r \\ & + 3k\frac{\mathrm{e}^{-2\mathbf{s}r^2}}{r}\sqrt{g_1(r)} + n\frac{\mathrm{e}^{\frac{\mathbf{s}r^2}{2}}}{r}\sqrt{g_1(r)}\Big).\end{aligned} \tag{12}$$

It is easy to observe that the first term is divergent. Hence, we obtain the potential energy according to $E = S/t$ after normalization as follows:

$$E_{QQq} = g\Big(2\int_0^{r_v}\Big(w(r)\sqrt{g_1(r)(\partial_r x)^2+g_2(r)}-\frac{1}{r^2}\Big)\mathrm{d}r-\frac{2}{r_v} + \int_{r_v}^{r_q} w(r)\sqrt{g_2(r)}\mathrm{d}r + 3k\frac{\mathrm{e}^{-2\mathrm{s}r_v^2}}{r_v}\sqrt{g_1(r_v)}+n\frac{\mathrm{e}^{\frac{\mathrm{s}r_q^2}{2}}}{r_q}\sqrt{g_1(r_q)}\Big)+2c. \tag{13}$$

where r_v denotes the independent variable at fixed T and η. By substituting the first term of the unnormalized energy into the Euler-Lagrange equation, we obtain:

$$\mathcal{H} = \frac{w(r)g_1(r)\partial_r x}{\sqrt{g_1(r)(\partial_r x)^2+g_2(r)}}, \tag{14}$$

Given that $\mathcal{H}$ is a constant, we obtain the following.

$$\mathcal{H}|_{r=r_v} = \frac{w(r_v)g_1(r_v)\cot(\alpha)}{\sqrt{g_1(r_v)\cot^2(\alpha)+g_2(r_v)}}. \tag{15}$$

According to $\mathcal{H}=\mathcal{H}|_{r=r_v}$,

$$\partial_r x = \sqrt{\frac{w(r_v)^2 g_1(r_v)^2 g_2(r)}{w(r)^2 g_1(r)^2\big(g_1(r_v)+g_2(r_v)\tan^2(\alpha)\big)-g_1(r)w(r_v)^2 g_1(r_v)^2}}. \tag{16}$$

Now, we determine the position of the light quark r_q and angle α between the string and x-axis at the baryon vertex. The generalized force equilibrium equations at the baryon vertex and light quark must be equal to zero. First, we consider the variation of their respective action quantities to obtain their generalized forces as follows:

$$e_1 = gw(r_v)\Big(-\sqrt{\frac{g_1(r_v)f(r_v)}{f(r_v)+\tan^2\alpha}},-\sqrt{\frac{g_1(r_v)}{f(r_v)^2\cot^2(\alpha)+f(r_v)}}\Big), \tag{17}$$

$$e_2 = gw(r_v)\Big(\sqrt{\frac{g_1(r_v)f(r_v)}{f(r_v)+\tan^2\alpha}},-\sqrt{\frac{g_1(r_v)}{f(r_v)^2\cot^2(\alpha)+f(r_v)}}\Big), \tag{18}$$

$$e_3 = gw(r_v)\big(0,\ \sqrt{g_2(r_v)}\big), \tag{19}$$

$$e_3' = gw(r_q)\big(0,-\sqrt{g_2(r_q)}\big), \tag{20}$$

$$f_q = \Big(0,-gn\partial_{r_q}\Big(\frac{\mathrm{e}^{\frac{\mathrm{s}r_q^2}{2}}}{r_q}\sqrt{g_1(r_q)}\Big)\Big), \tag{21}$$

$$f_v = \Big(0,-3gk\partial_{r_v}\Big(\frac{\mathrm{e}^{-2\mathrm{s}r_v^2}}{r_v}\sqrt{g_1(r_v)}\Big)\Big), \tag{22}$$

where e_i denotes the string tension, and f_q and f_v denote the forces provided by the light quark and baryon vertices, respectively [20].

It is evident that the generalized force equilibrium equation at the light quark is solely a function of r_q and can be expressed as follows:

$$F_1(r_q) = \frac{f_q+e_3'}{gw(r_q)} = 0. \tag{23}$$

Additionally, we can solve for r_q based on this equation by changing T and η. The force balance equation at the vertex is as follows:

$$f_v+e_3+e_1+e_2 = 0. \tag{24}$$

In addition to T and η, the equation has only two unknowns, r_v and α, By solving the equation, we can obtain the function of α as a function of r_v. Then, we can express distance L as a function of r_v:

$$L = 2\int_0^{r_v}\frac{\partial x}{\partial r}\mathrm{d}r. \tag{25}$$

Together with Eqs. (13) and (25), we can numerically solve the energy at small L.

B. Intermediate L

According to Fig. 2, when compared to small L, intermediate L is only missing a straight string from r_v to r_q, and the sum of the action can be expressed as

$$S = \sum_{i=1}^{2} S_{\mathrm{NG}}^{(i)} + S_{\mathrm{vert}} + S_q. \tag{26}$$

We chose the same static gauge as selected earlier. It is easy to show that the sum of Nambu-Goto action becomes:

$$\sum_{i=1}^{2} S_{\mathrm{NG}}^{(i)} = 2g\int_0^t \mathrm{d}t\int_0^{r_v} w(r)\sqrt{g_1(r)(\partial_r x)^2+g_2(r)}\mathrm{d}r. \tag{27}$$

Then, the boundary condition becomes:

$$x(0) = \pm\frac{L}{2},\ \ x(r_v)=0,\ \ (\partial_r x|_{r=r_v})^2 = \cot^2(\alpha). \tag{28}$$

Therefore, the potential energy can be expressed as

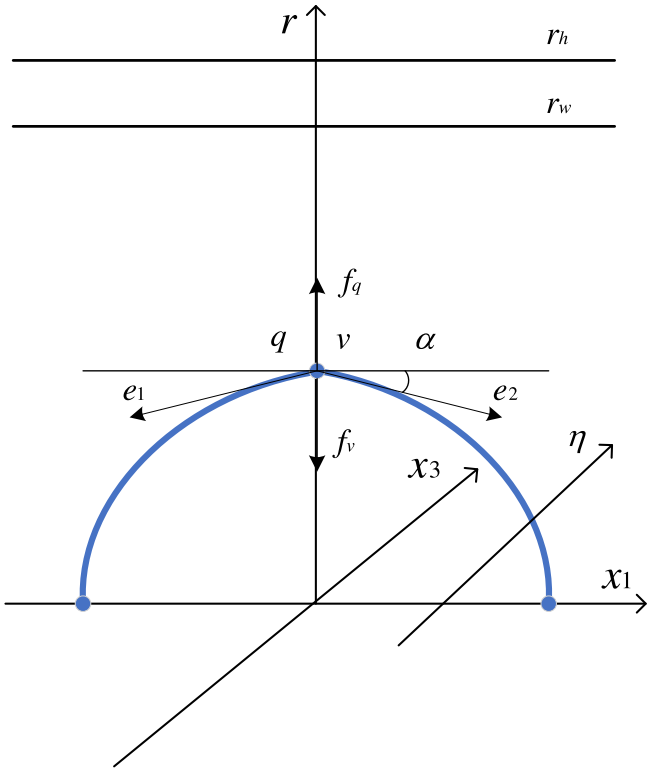

Fig. 2. (color online) String configuration at an intermediate separation distance of a heavy quark pair. We use the straight line between two heavy quarks Q as x_1-axis, and baryon vertex and light quarks are in the same position on the r-axis. Rapidity η is along x_3-axis direction. The black arrows represent generalized forces. Furthermore, r_h denotes the position of the black hole horizon. Additionally, r_w denotes the position of an imaginary wall when QQq is confined.

$$E_{QQq} = g\Big(2\int_0^{r_v}\Big(w(r)\sqrt{g_1(r)(\partial_r x)^2+g_2(r)}-\frac{1}{r^2}\Big)\mathrm{d}r-\frac{2}{r_v} + 3k\frac{\mathrm{e}^{-2sr_v^2}}{r_v}\sqrt{g_1(r_v)}+n\frac{\mathrm{e}^{\frac{sr_v^2}{2}}}{r_v}\sqrt{g_1(r_v)}\Big)+2c. \tag{29}$$

Finally, we can write the equation for the equilibrium of generalized force at the coincidence of the light quark and the baryon vertex as

$$f_v + f_q + e_1 + e_2 = 0, \tag{30}$$

and each force can be expressed as

$$e_1 = gw(r_v)\Big(-\sqrt{\frac{g_1(r_v)f(r_v)}{f(r_v)+\tan^2\alpha}}, -\sqrt{\frac{g_1(r_v)}{f(r_v)^2\cot^2(\alpha)+f(r_v)}}\Big), \tag{31}$$

$$e_2 = gw(r_v)\Big(\sqrt{\frac{g_1(r_v)f(r_v)}{f(r_v)+\tan^2\alpha}}, -\sqrt{\frac{g_1(r_v)}{f(r_v)^2\cot^2(\alpha)+f(r_v)}}\Big), \tag{32}$$

$$f_q = \Big(0, -gn\partial_{r_v}\Big(\frac{\mathrm{e}^{\frac{sr_v^2}{2}}}{r_v}\sqrt{g_1(r_v)}\Big)\Big), \tag{33}$$

$$f_v = \Big(0, -3gk\partial_{r_v}\Big(\frac{\mathrm{e}^{-2sr_v^2}}{r_v}\sqrt{g_1(r_v)}\Big)\Big). \tag{34}$$

According to Eqs. (25) and (29), we can obtain the energy at intermediate L:

C. Large L

As observed in Fig. 3, the configuration comprises two strings, the vertex, and the light quark. However, due to the presence of smooth turning points on the strings, we can utilize a new static gauge that simplifies the calculations. In this gauge, we set $\xi^0 = t, \xi^1 = x$, and consider r as a function of x. Accordingly, we can express the total action as follows:

$$S = gt\Big(\int_{-\frac{L}{2}}^{0} w(r)\sqrt{g_1(r)+g_2(r)(\partial_x r)^2}\mathrm{d}x + \int_0^{\frac{L}{2}} w(r)\sqrt{g_1(r)+g_2(r)(\partial_x r)^2}\mathrm{d}x + 3k\frac{\mathrm{e}^{-2sr^2}}{r}\sqrt{g_1(r)}+n\frac{\mathrm{e}^{\frac{sr^2}{2}}}{r}\sqrt{g_1(r)}\Big). \tag{35}$$

Furthermore, the boundary condition of $r(x)$ is as follows:

$$r\Big(\pm\frac{L}{2}\Big) = 0, r(0) = r_v, \begin{cases}(\partial_x r)^2 = \tan^2(\alpha), & r = r_v\\ (\partial_x r)^2 = 0, & r = r_0.\end{cases} \tag{36}$$

The generalized force balance equation at r_v is the same as for intermediate L. We can use this equation to relate r_v to α. Additionally, we need to find the functional relationship between r_0 and r_v due to inflection points. To accomplish this, we can employ the Euler-Lagrange equation and incorporate the action of the string to derive the first integral.

$$\mathcal{H} = \frac{w(r)g_1(r)}{\sqrt{g_1(r)+g_2(r)(\partial_x r)^2}}, \tag{37}$$

$\mathcal{H}$ is a constant. We bring the boundary conditions to the first integral.

$$\mathcal{H}|_{r=r_v} = \frac{w(r_v)g_1(r_v)}{\sqrt{g_1(r_v)+g_2(r_v)\tan^2(\alpha)}}, \tag{38}$$

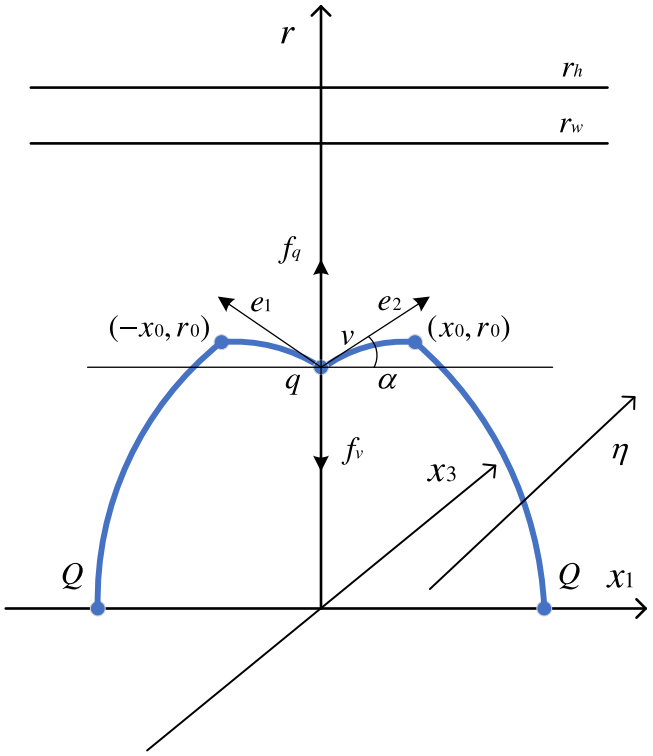

Fig. 3. (color online) String configuration at a large separation distance of a heavy quark pair. We use the straight line between two heavy quarks Q as the x_1-axis, and baryon vertex and light quarks are in the same position on the r-axis. The rapidity η is along the x_3-axis direction. There is a smooth turning point on each of the two strings. The black arrows represent generalized forces. r_h denotes the position of the black hole horizon. r_w denotes the position of an imaginary wall when the QQq is confined.

$$\mathcal{H}|_{r=r_0} = w(r_0)\sqrt{g_1(r_0)}. \tag{39}$$

Hence, we obtain

$$\partial_x r = \sqrt{\frac{w(r)^2 g_1(r)^2 - g_1(r) w(r_0)^2 g_1(r_0)}{w(r_0)^2 g_1(r_0) g_2(r)}}. \tag{40}$$

Given that the correspondence between α and r_v has been established in the generalized force equilibrium equation, we can determine the correspondence between r_0 and r_v by using the following relationship:

$$w(r_0)\sqrt{g_1(r_0)} = \frac{w(r_v) g_1(r_v)}{\sqrt{g_1(r_v) + g_2(r_v)\tan^2(\alpha)}}. \tag{41}$$

Furthermore, $\partial_r x = \dfrac{1}{\partial_x r}$. To simplify the calculations, we can obtain the energy after performing the integral equivalent transformation and renormalization as follows:

$$\begin{aligned} E_{QQq} = g\Big(2\int_0^{r_v}\Big(w(r)\sqrt{g_1(r)(\partial_r x)^2 + g_2(r)} - \frac{1}{r^2}\Big)\mathrm{d}r \\ + 2\int_{r_v}^{r_0} w(r)\sqrt{g_1(r)(\partial_r x)^2 + g_2(r)}\mathrm{d}r \\ - \frac{2}{r_v} + 3k\frac{\mathrm{e}^{-2s r_v^2}}{r}\sqrt{g_1(r_v)} + n\frac{\mathrm{e}^{\frac{s r_v^2}{2}}}{r_v}\sqrt{g_1(r_v)}\Big) + 2c. \end{aligned} \tag{42}$$

Referring to Fig. 3, the separation distance of the heavy-quark pair L should be:

$$L = 2\Big(\int_0^{r_v}\frac{\partial x}{\partial r}\mathrm{d}r + \int_{r_v}^{r_0}\frac{\partial x}{\partial r}\mathrm{d}r\Big). \tag{43}$$

Combining Eqs. (42) and (43), we can obtain the potential energy at large L.

III. NUMERICAL RESULTS

At low temperatures and low rapidities, QQq is confined, and there is an imaginary wall r_w [58–62]. However, as the temperature or rapidity increases, QQq will also become deconfined. When QQq is confined, the separation distance L and potential energy E will increase with r_v. Furthermore, at a certain point, L will increase sharply until infinity. However, in reality, the separation distance L does not continue to increase infinitely. When the potential energy of QQq reaches a certain critical point, the string connecting the quarks breaks, which is termed as string breaking. This leads to the excitation of light and anti-light quarks in the vacuum. When the QQq is deconfined, the imaginary wall disappears. As r_v increases, the separation distance reaches a maximum, and simultaneously, the potential energy reaches a maximum at this point. This implies QQq screening at this point.

This section examines the properties of QQq at finite rapidity based on different research perspectives. It can be divided into three parts. First, it involves analyzing the influence of rapidity on the string breaking of the confined state. Second, it involves investigating the effect of screening when the QQq is deconfined. Finally, it involves conducting a comprehensive comparison with $Q\bar{Q}$. Additionally, we construct a state diagram of QQq and $Q\bar{Q}$ in the $T-\eta$ plane to graphically represent their behavior.

Based on Eq. (23), we can solve for the light quark position corresponding to (T,η). There are two solutions to this equation within the valid interval, and only the smaller solution satisfies our requirements. We consider this equation as a function of r_q with different T and η shown in Fig. 4. We solve for r_q in these cases at $T = 0.1$ GeV and obtain the following results: $\eta = 0.3$, $r_q = 1.1487\ \mathrm{GeV}^{-1}$; $\eta = 0.6$, $r_q = 1.1587\ \mathrm{GeV}^{-1}$; $\eta = 0.9$, $r_q = 1.1823\ \mathrm{GeV}^{-1}$; $\eta = 1.3865$, $r_q = 1.4582\ \mathrm{GeV}^{-1}$.

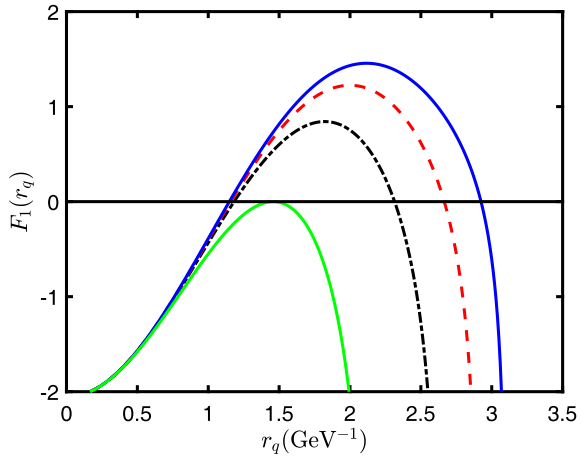

Fig. 4. (color online) F_1 as a function of r_q for various rapidities at $T = 0.1\,\mathrm{GeV}$. The blue line represents $\eta = 0.3$, the red dashed line represents $\eta = 0.6$, the black dot-dashed line represents $\eta = 0.9$, and the green line represents $\eta = 1.3865$. Only the green line has one zero point, and the other three lines have two zero points.

In Fig. 4, it can be observed that, at a constant temperature, the function $F_1(r_q)$ decreases as the rapidity increases until it no longer has any zero values. For each temperature value, there is a corresponding rapidity that results in the function having exactly one solution. We can obtain solutions by solving the following equations:

$$\begin{cases} F_1(r_q, T, \eta) & = 0, \\ \dfrac{\partial F_1(r_q, T, \eta)}{\partial r_q} & = 0. \end{cases} \tag{44}$$

We calculate the angle at different rapidities using Eq. (24) as a function of r_v at a temperature of $T = 0.1$ GeV. The resulting plot is shown in Fig. 5. It is evident that regardless of the parameters, the angles are always greater than zero, and as the rapidity increases, the angle decreases. The transverse axes of the angles all start at zero and end at their respective light quark positions r_q. When the baryon vertex coincides with the light quark, denoted by $r_v = r_q$, it indicates that the configuration has entered the second stage, which corresponds to intermediate L. Subsequently, the light quark and baryon vertex increase together. Specifically, the stage where $r_v < r_q$ is referred to as the first stage, termed as small L.

At the intermediate L, we can solve Eq. (30) to obtain the relation between angles α and r_v. Then, we draw this plot at different rapidities, as shown in Fig. 6. It can be observed that, when the rapidity is small, the angle decreases with r_v linearly, and when it decreases to less than 0, we consider that QQq transitions from the second stage to the third stage, which corresponds to large L. Additionally, as the rapidity increases, the angular plot of the

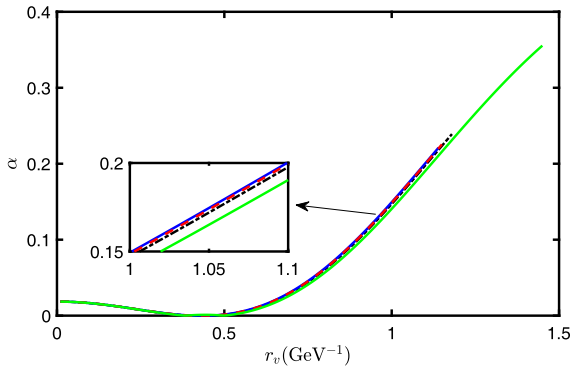

Fig. 5. (color online) Relation between the position r_v of the baryon vertex and angle α, which is between the string and horizon at $T = 0.1\,\mathrm{GeV}$ and various rapidities. Among them, the blue line represents $\eta = 0.3$, the red dashed line represents $\eta = 0.6$, the black dot-dashed line represents $\eta = 0.9$, and the green line represents $\eta = 1.3865$.

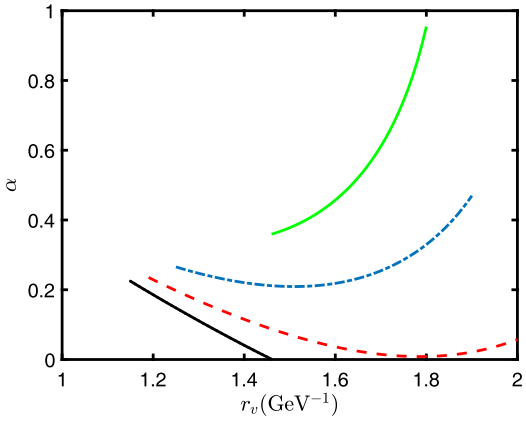

Fig. 6. (color online) Relation between the position r_v of the baryon vertex and angle α, which is between the string and horizontal at $T = 0.1\,\mathrm{GeV}$ and various rapidities. Among them, the black line represents $\eta = 0.3$, the red dashed line represents $\eta = 0.9$, the blue dot-dashed line represents $\eta = 1.2$, and the green line represents $\eta = 1.3865$.

second stage changes significantly. The curve of α always moves upwards, does not continue to monotonically decrease, and gradually bends upwards from a straight line to a curve. Hence, ultimately it monotonically increases. Based on these results, when the rapidity is large, the third stage configuration of the model is not possible.

Figure 7 shows the relation between angles α and the r_v in the third stage. This result is obtained through Eq. (30). Their transverse axes all start at the end point of their respective second stages, and the longitudinal axes start at 0. It can be seen that, as the rapidity increases, the range of configuration in the third stage continues to decrease until it no longer exists. This dovetails with our analysis in the second phase. Since the string configura-

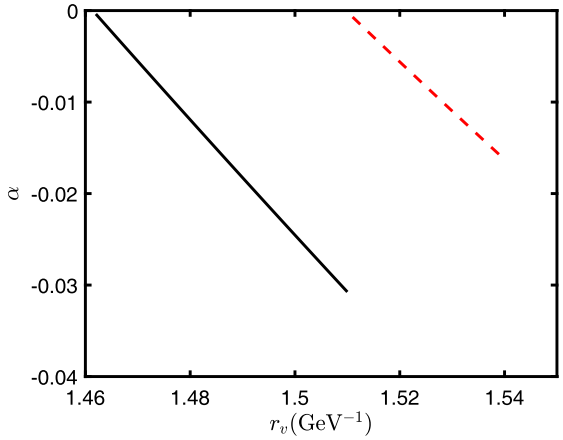

Fig. 7. (color online) Relation between the position r_v of the baryon vertex and angle α, which is between the string and horizontal, at $T = 0.1\,\mathrm{GeV}$ and various rapidities. Among them, the black line represents $\eta = 0.3$; the red dashed line represents $\eta = 0.6$.

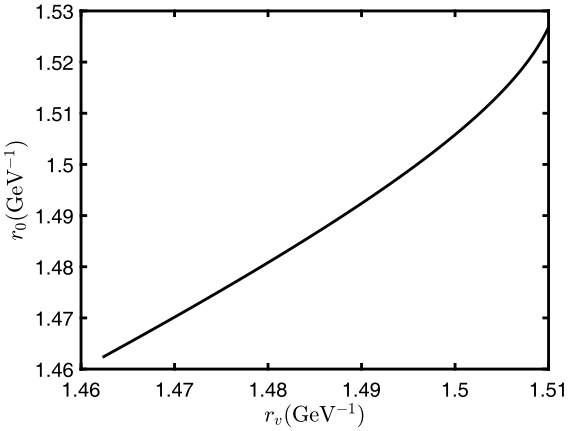

Fig. 8. Relation between the smooth turning point r_0 on the string and position r_v of the baryon vertex at $T = 0.1\,\mathrm{GeV}$ and $\eta = 0.3$.

tion features smooth turning points during the third stage, we obtain the relation between r_v and r_0 using Eq. (41), as shown in Fig. 8. From the calculated results between α and r_v in each stage, it can be observed that α is smooth between the two stages.

In Fig. 9, we present the results of L as a function of r_v based on Eqs. (25) and (43). At $T = 0.1\,\mathrm{GeV}$ and $\eta = 0.3$, QQq will be confined, and the separation distance can tend to infinity. Subsequently, we use Eqs. (13), (29), and (42) to obtain a plot of E and L as shown in Fig. 10. In the confined state, the potential of QQq is also the Cornell potential with finite temperature and rapidity.

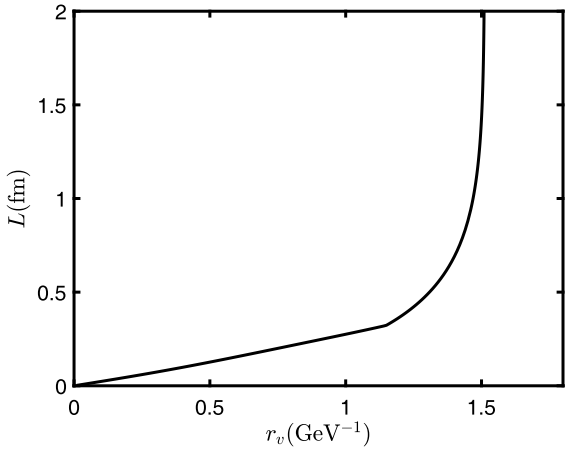

Fig. 9. Separation distance L between pairs of heavy quarks as a function of the position r_v of the baryon vertex at $T = 0.1\,\mathrm{GeV}$ and $\eta = 0.3$.

A. Confined state

When QQq is confined, string breaking occurs when potential energy E reaches a certain value, exciting positive and negative light quarks in the vacuum. The pattern of string breaking is as follows:

$$QQq \longrightarrow Qqq + Q\bar{q}. \tag{45}$$

The schematic diagram after the string breaking is shown in Fig. 11. It can be observed that the action of Qqq is provided by three strings, a baryon vertex, and two light quarks. The action of $Q\bar{q}$ comprises a string and light quark. Therefore, the total action after the string breaking is as follows:

$$S_{Qqq} = \sum_{i=1}^{3} S_{\mathrm{NG}}^{(i)} + S_{\mathrm{vert}} + 2S_q, \tag{46}$$

$$S_{Q\bar{q}} = S_{\mathrm{NG}} + S_q. \tag{47}$$

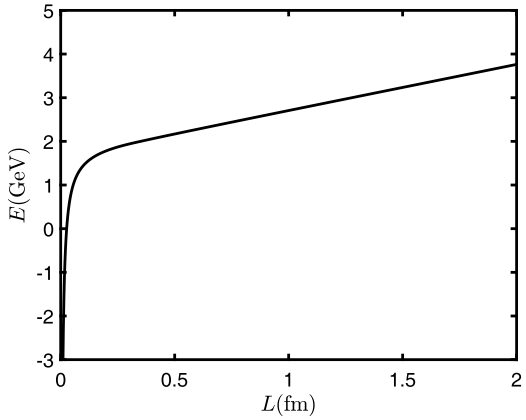

Fig. 10. Relation between QQq potential energy E and heavy-quark pair separation distance L at $T = 0.1\,\mathrm{GeV}$ and $\eta = 0.3$.

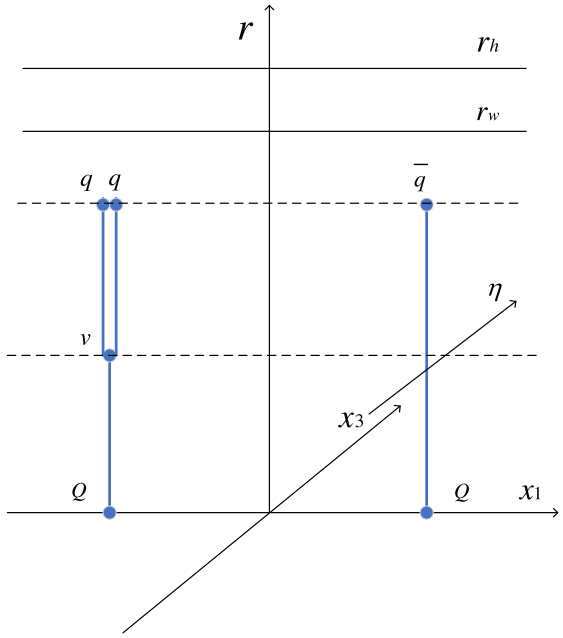

Fig. 11. (color online) Schematic diagram after string breaking. Rapidity η is along the x_3-axis direction. r_h denotes the position of the black hole horizon. r_w denotes the position of an imaginary wall when QQq is confined.

We select the gauge as $\xi^0 = t, \xi^1 = r$. Therefore, we obtain that the boundary condition of $x(r)$ is as follows:

$$(\partial_r x)^2 = 0. \tag{48}$$

Hence, the total action can be expressed as

$$\begin{aligned} S = gt\Big(& \int_0^{r_v} w(r)\sqrt{g_2(r)}\mathrm{d}r + 2\int_{r_v}^{r_q} w(r)\sqrt{g_2(r)}\mathrm{d}r \\ & + \int_0^{r_q} w(r)\sqrt{g_2(r)}\mathrm{d}r \\ & + 3k\frac{\mathrm{e}^{-2sr_v^2}}{r_v}\sqrt{g_1(r_v)} + 3n\frac{\mathrm{e}^{\frac{sr_q^2}{2}}}{r_q}\sqrt{g_1(r_q)}\Big). \end{aligned} \tag{49}$$

A simple analysis shows that the generalized force equilibrium equation at light quarks does not change after string breaking, i.e., the positions of the three light quarks will be consistent with the one before breaking. However, the force configuration at the baryon vertex of Qqq changes, and we can denote it as follows:

$$F_2(r_v) = \frac{2e_3 - e_3 + f_v}{gw(r_v)} = \frac{e_3 + f_v}{gw(r_v)} = 0, \tag{50}$$

where e_3 and f_v coincide with Eqs. (19) and (22). There is only one unknown quantity, r_v, in the aforementioned equation, Hence, we can solve for its value. This equation usually solves for two values within the range where r_v has physical significance, and we consider the smaller value here. We solve for r_v in these cases at $T = 0.1$ GeV as follows: $\eta = 0.3$, $r_v = 0.4088\,\mathrm{GeV}^{-1}$; $\eta = 0.6$, $r_v = 0.4049\,\mathrm{GeV}^{-1}$; $\eta = 0.9$, $r_v = 0.3987\,\mathrm{GeV}^{-1}$.

Then, we consider the renormalization to determine the potential energy after string breaking:

$$\begin{aligned} E_{\mathrm{break}} = g\Big(& \int_0^{r_v} \Big(w(r)\sqrt{g_2(r)} - \frac{1}{r^2}\Big)\mathrm{d}r \\ & + 2\int_{r_v}^{r_q} w(r)\sqrt{g_2(r)}\mathrm{d}r + \int_0^{r_q} \Big(w(r)\sqrt{g_2(r)} - \frac{1}{r^2}\Big)\mathrm{d}r \\ & - \frac{1}{r_v} - \frac{1}{r_q} + 3k\frac{\mathrm{e}^{-2sr_v^2}}{r_v}\sqrt{g_1(r_v)} + 3n\frac{\mathrm{e}^{\frac{sr_q^2}{2}}}{r_q}\sqrt{g_1(r_q)}\Big) + 2c. \end{aligned} \tag{51}$$

We calculate the potential energy at $T = 0.1$ GeV after string breaking and obtain the following: $\eta = 0.3$, $E_{\mathrm{break}} = 3.0040$ GeV; $\eta = 0.6$, $E_{\mathrm{break}} = 2.9983$ GeV; $\eta = 0.9$, $E_{\mathrm{break}} = 2.9857$ GeV.

The potential energies of QQq are shown in Fig. 12. From Fig. 12, it can be observed that a higher rapidity leads to a lower potential energy of QQq. The calculated data are as follows: $\eta = 0.3$, $L_{\mathrm{break}} = 1.2812$ fm; $\eta = 0.6$, $L_{\mathrm{break}} = 1.2874$ fm; $\eta = 0.9$, $L_{\mathrm{break}} = 1.3037$ fm. Based on these results, we conclude that the string-breaking distance is enhanced and potential energy is decreased in the presence of increased rapidity.

B. Deconfined state

The confined or deconfined state of the QQq can be determined by analyzing the plots of $L - r_v$ and the effective string tension. It has been observed that the results obtained from both methods are consistent [61]. We calculate the plots of $L - r_v$ for different rapidities at the same

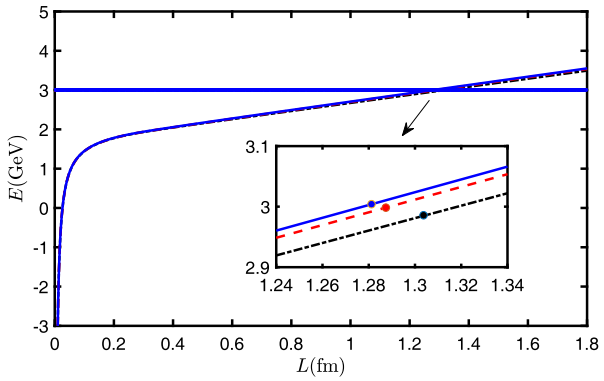

Fig. 12. (color online) Curves in the figure are the potential energy of QQq at $T = 0.1$ GeV, and the straight lines denote the potential energy at $T = 0.1$ GeV after string breaking. The black dot-dashed line represents $\eta = 0.9$. The red dashed line represents $\eta = 0.6$. The blue solid line represents $\eta = 0.3$.

temperature, as shown in Fig. 13. As the separation distance L of the QQq increases, it approaches infinity. In contrast, when it is deconfined, the $L-r_v$ plot has a maximum value. Specifically, QQq will become free quarks above the maximum value.

Figure 13 illustrates the transition of the QQq from a confined to a deconfined state at a critical rapidity and temperature. When QQq is deconfined, it is observed that, as the rapidity increases, the screening distance and r_v decrease. This implies that, as the rapidity increases, QQq becomes easier to screen. When $T=0.1\,\text{GeV}$, $\eta=1.3865$ is the maximum rapidity that the QQq model

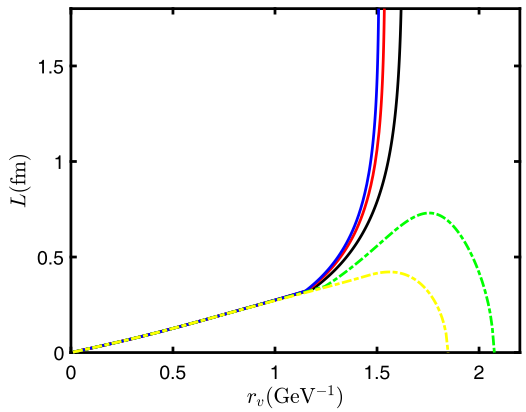

Fig. 13. (color online) Separation distance L between pairs of heavy quarks as a function of the position r_v of the baryon vertex at $T=0.1\,\text{GeV}$. The solid line represents in confined state, while the dashed line represents in deconfined state. The blue line represents $\eta=0.3$, the red line represents $\eta=0.6$, the black line represents $\eta=0.9$, the green line represents $\eta=1.2$, and the yellow line represents $\eta=1.3865$.

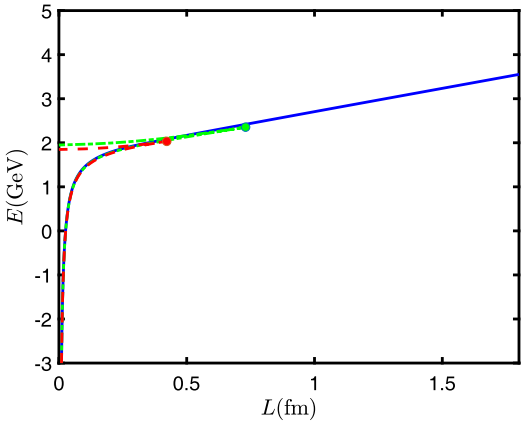

Fig. 14. (color online) Relation between the potential energy E and separation distance L at $T=0.1\,\text{GeV}$. The solid line represents a confined state, while the dashed line represents a deconfined state. The solid blue line represents $\eta=0.3$, the green dot-dashed line represents $\eta=1.2$, and the red dashed line represents $\eta=1.3865$.

can allow, and its corresponding screening distance is $L_{\text{melt}}=0.4218\,\text{fm}$. Then, $r_v=1.5682\,\text{GeV}^{-1}$.

We also calculate the plots of E and L as shown in Fig. 14. Based on the figure, it can be observed that the potential energy of the confined QQq steadily increases with L until string breaking occurs. There is a maximum value for the potential energy of the deconfined state. When E reaches the maximum value, L also reaches the maximum value, which is the apex of L in Fig. 13. As rapidity increases, the potential energy of QQq decreases, and the screening distance becomes smaller. Figure 14 also illustrates that, regardless of whether it is in the confined or deconfined state, as the rapidity increases at a fixed temperature, the potential energy becomes smaller. The calculation results about the screening of QQq in the deconfined state are as follows: at $\eta=1.2$, $L_{\text{screen}}=0.7304$ fm, $E_{\text{screen}}=2.3547$ GeV; at $\eta=1.3865$, $L_{\text{screen}}=0.4219$ fm, $E_{\text{screen}}=2.0317$ GeV.

We will briefly introduce the method for determining confined and deconfined states. If the maximum value of the screening distance is smaller than the distance of string breaking, it indicates that QQq is in the deconfined state; otherwise, it is in the confined state. Using this method, we perform calculations to determine the critical points, and these results are plotted in Fig. 15.

In Fig. 15, QQq cannot exist in a medium with temperatures and rapidities above the dashed line. Specifically, QQq is in the deconfined state between the dashed and solid lines. In this state, QQq become free quarks at long distances due to screening. When QQq is in the deconfined state and the rapidity increases at a fixed temperature, the screening distance decreases. Below the solid line, QQq is in the confined state. In this state, when the separation distance reaches the string-breaking distance and string breaking occurs, it transitions into a new configuration.

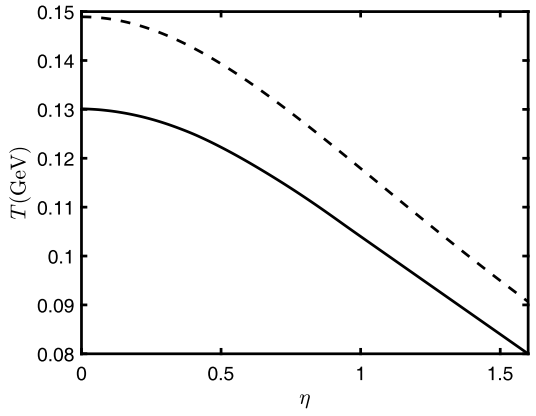

Fig. 15. (color online) Dashed line consists of the maximum (η, T) points determined via Eq. (44), and the solid line consists of the critical points that distinguish the confined state from the deconfined state.

C. Comparison with $Q\bar{Q}$ configuration

Research on $Q\bar{Q}$ through holographic models is sufficiently mature [46, 62−69]. We mainly examine the difference between $Q\bar{Q}$ and QQq under the influence of rapidities.

First, we can write the metric after adding the rapidity effect of $Q\bar{Q}$ through the Lorentz transformation:

$$\begin{aligned} ds^2 = w(r)\Big(&- g_1(r)dt^2 - 2\sinh(\eta)\cosh(\eta)\big(1-\frac{g_1(r)}{g_2(r)}\big)dx_3dt \\ &+ g_3(r)dx_3^2 + dx_1^2 + dx_2^2 + \frac{g_2(r)}{g_1(r)}dr^2\Big), \end{aligned} \tag{52}$$

where $w(r), g_1(r), g_2(r)$, and $g_3(r)$ are consistent with the previously derived Eqs. (2) and (5).

We select the static gauge $\xi^0 = t$, $\xi^1 = x$, and the action of $Q\bar{Q}$can be expressed as

$$\begin{aligned} S = gt\Big(&\int_{-\frac{L}{2}}^{0} w(r)\sqrt{g_1(r)+g_2(r)(\partial_x r)^2}dx \\ &+ \int_{0}^{\frac{L}{2}} w(r)\sqrt{g_1(r)+g_2(r)(\partial_x r)^2}\Big)dx. \end{aligned} \tag{53}$$

Furthermore, the boundary condition of $r(x)$ is as follows:

$$r\Big(\pm\frac{L}{2}\Big) = 0,\ \ r(0) = r_0,\ \ (\partial_x r|_{r=r_0})^2 = 0. \tag{54}$$

The string configuration of $Q\bar{Q}$ is U-shaped, where r_0 denotes the smooth turning point of the U-shaped string. With the Euler-Lagrange equation, we obtain the following:

$$\partial_x r = \sqrt{\frac{w(r)^2 g_1(r)^2 - g_1(r)w(r_0)^2 g_1(r_0)}{w(r_0)^2 g_1(r_0)g_2(r)}}. \tag{55}$$

By renormalizing, we can obtain the potential energy of $Q\bar{Q}$as follows:

$$\begin{aligned} E_{Q\bar{Q}} = g\Big(2\int_0^{r_0}\big(w(r)\sqrt{g_1(r)(\partial_r x)^2+g_2(r)}-\frac{1}{r^2}\big)dr \\ -\frac{2}{r_0}\Big) + 2c. \end{aligned} \tag{56}$$

Furthermore,

$$L = 2\int_0^{r_0}\frac{\partial x}{\partial r}dr, \tag{57}$$

where $\partial_r x = \dfrac{\partial x}{\partial r} = \dfrac{1}{\partial_x r}$.

We can calculate the potential energy of $Q\bar{Q}$ at different rapidities at the same temperature and compare it with QQq. The result is presented in Fig. 16, indicating that the potential energy of QQq is higher than that of $Q\bar{Q}$. Furthermore, it is observed that increasing rapidity consistently leads to a decrease in the potential energy of $Q\bar{Q}$ and QQq. When $Q\bar{Q}$ is in the confined state, the $Q\bar{Q}$ string breaks when the separation distance becomes sufficiently large. Let us consider the pattern of $Q\bar{Q}$ string breaking as

$$Q\bar{Q} \longrightarrow Q\bar{q} + \bar{Q}q. \tag{58}$$

Evidently,

$$\begin{aligned} E_{break} = 2g\Big(&\int_0^{r_q}\big(w(r)\sqrt{g_2(r)}-\frac{1}{r^2}\big)dr \\ &-\frac{1}{r_q}+n\frac{e^{\frac{sr_q^2}{2}}}{r_q}\sqrt{g_1(r_q)}\Big)+2c. \end{aligned} \tag{59}$$

Based on this, we can generate the plot in Fig. 17. As shown in the figure, it is evident that increasing rapidity leads to a greater separation distance at the point of string breaking for both $Q\bar{Q}$ and QQq. The calculated data are $\eta = 0.3, E_{\rm break} = 2.3906$ GeV, $L_{\rm break} = 1.2331$ fm; $\eta = 0.6$, $E_{\rm break} = 2.3868$ GeV, $L_{\rm break} = 1.2382$ fm; $\eta = 0.9$, $E_{\rm break} = 2.3784$ GeV, $L_{\rm break} = 1.2474$ fm. It can be observed that the breaking distance of $Q\bar{Q}$ is slightly less than QQq. However, the difference between the two is not significant.

When the rapidity continues to increase, $Q\bar{Q}$ will also change from the confined state to the deconfined state. For this purpose, we calculated the results in Fig. 18. When we calculated the potential of QQq at $\eta = 1.3865$ and $T = 0.1$ GeV, the results show $L_{\rm melt} = 0.4219$ fm and $E_{\rm melt} = 2.0317$ GeV. When $Q\bar{Q}$ is at $\eta = 1.3865$ and

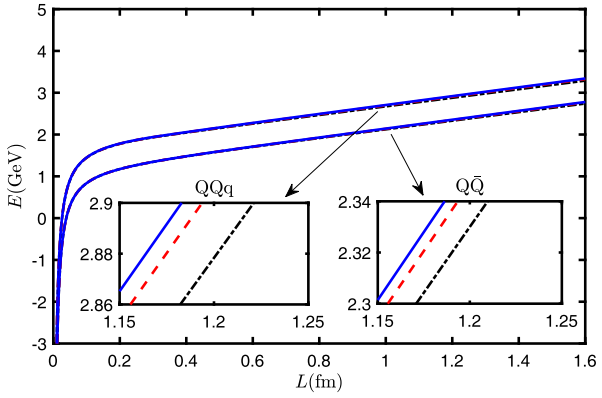

Fig. 16. (color online) Potential energies of $Q\bar{Q}$ and QQq are depicted at $T = 0.1$ GeV. In the graph, the black dot-dashed line represents $\eta = 0.9$, the red dashed line represents $\eta = 0.6$, and the blue solid line represents $\eta = 0.3$.

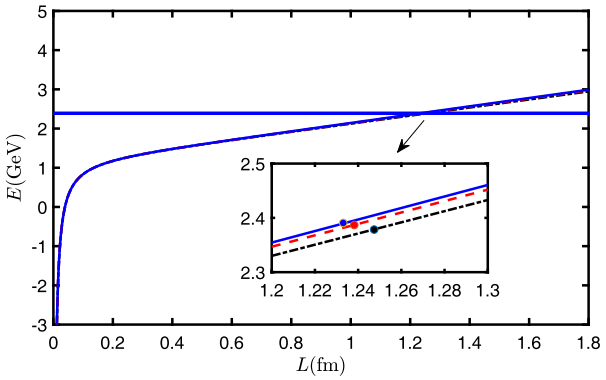

Fig. 17. (color online) Curves in the figure are the potential energy of $Q\bar{Q}$ at $T = 0.1\,\mathrm{GeV}$, and the straight lines are the potential energy at $T = 0.1\,\mathrm{GeV}$ after string breaking. Where the black dot-dashed line represents $\eta = 0.9$, the red dashed line represents $\eta = 0.6$, and the blue solid line represents $\eta = 0.3$.

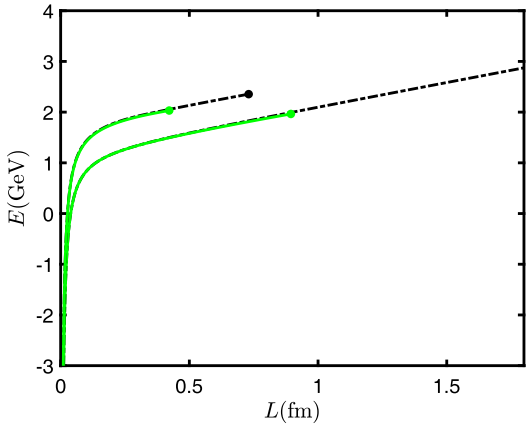

Fig. 18. (color online) Higher curves represent QQq, and the lower curves represent $Q\bar{Q}$. The black line represents $\eta = 1.2, T = 0.1\,\mathrm{GeV}$, and the green line represents$\eta = 1.3865$, $T = 0.1$ GeV.

$T = 0.1$ GeV, we obtain $L_{\mathrm{melt}} = 0.8944$ fm and $E_{\mathrm{melt}} = 1.9640$ GeV. It can be observed that the difference in screening distances is significant. We infer that $Q\bar{Q}$ is more stable than QQq at the same temperature and rapidity.

Figure 19 shows that QQq is confined below the black line, which implies that the separation distance of heavy quarks can be infinite if we ignore the string breaking. QQq can still be found below the black dashed line even when QQq is in the deconfined state. This implies that QQq can screen at a certain distance. Furthermore, QQq cannot be found anymore above the dashed line. As a comparison, we show $Q\bar{Q}$ in the same figure with a blue line. The situation differs for $Q\bar{Q}$. Additionally, $Q\bar{Q}$ is confined below the blue line. Above the blue line, $Q\bar{Q}$ is deconfined. However, we can still find $Q\bar{Q}$ at any conditions because it can still exist at a small separation distance.

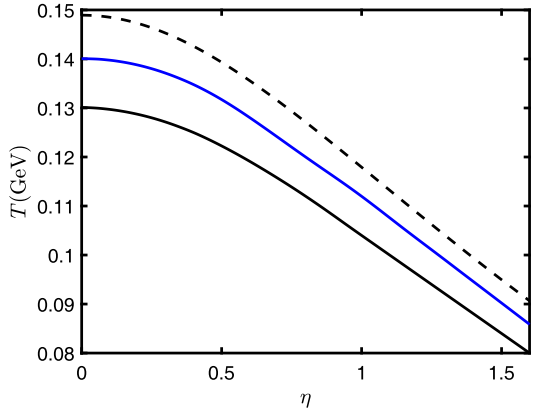

Fig. 19. (color online) Solid black line distinguishes the confined state and deconfined state of QQq, the dashed line represents the maximum conditions allowed by QQq, the blue line distinguishes the confined state and deconfined state of $Q\bar{Q}$.

IV. CONCLUSION

In this paper, we mainly discuss the properties of QQq in some aspects at finite temperature and rapidity using the 5-dimensional effective string model for the first time. When QQq is in the confined state, it can undergo string breaking at a large separation distance. We consider the breaking mode to be $QQq \longrightarrow Qqq + Q\bar{q}$ and observe that higher rapidities make the string breaking more difficult to occur. Under high temperature and rapidity conditions, QQq transitions into the deconfined state. In this state, it becomes the free quarks if the separation distance is larger than the screening distance, and color screening becomes easier with increasing rapidity. Using potential analysis, we constructed a state diagram for QQq in the $T-\eta$ plane to differentiate between the confined and deconfined states.

We compared the properties of QQq and $Q\bar{Q}$. As expected, the potential energy of QQq is always greater than that of $Q\bar{Q}$, and the qualitative effects of temperature and rapidity on QQq and $Q\bar{Q}$ are consistent. In the confined state, it is determined that the string-breaking distance of QQq and $Q\bar{Q}$ are very close. This implies that the sizes of the different hadrons are potentially similar. In the deconfined state, there is a significant difference in the screening distance between QQq and $Q\bar{Q}$. It is determined that the screening distance of QQq is smaller than that of $Q\bar{Q}$ under the same conditions, which indicates QQq is less stable than $Q\bar{Q}$. Furthermore, an interesting result shows that QQq cannot be found above certain temperatures and rapidities. However, $Q\bar{Q}$ can be found at any temperature and rapidity as long as the separation distances are sufficiently small. This study mainly focuses on qualitative analysis and can be extended to yield more accurate results in the future.

References

[1] R. Aaij *et al.* (LHCb), Phys. Rev. Lett. **119**(11), 112001 (2017), arXiv:1707.01621[hep-ex]
[2] R. Aaij *et al.* (LHCb), Phys. Rev. Lett. **121**(16), 162002 (2018), arXiv:1807.01919[hep-ex]
[3] E. Eichten, K. Gottfried, T. Kinoshita *et al.*, Phys. Rev. D **21**, 203 (1980)
[4] A. Yamamoto, H. Suganuma, and H. Iida, Phys. Rev. D **78**, 014513 (2008), arXiv:0806.3554[hep-lat]
[5] J. Najjar and G. Bali, PoS **LAT2009**, 089 (2009), arXiv:0910.2824[hep-lat]
[6] J. M. Maldacena, Phys. Rev. Lett. **80**, 4859 (1998), arXiv:hep-th/9803002[hep-th]
[7] S. J. Rey, S. Theisen, and J. T. Yee, Nucl. Phys. B **527**, 171 (1998), arXiv:hep-th/9803135[hep-th]
[8] A. Brandhuber, N. Itzhaki, J. Sonnenschein *et al.*, Phys. Lett. B **434**, 36 (1998), arXiv:hep-th/9803137[hep-th]
[9] C. Alexandrou, P. de Forcrand, and O. Jahn, Nucl. Phys. B Proc. Suppl. **119**, 667 (2003), arXiv:hep-lat/0209062
[10] C. Alexandrou, P. De Forcrand, and A. Tsapalis, Nucl. Phys. B Proc. Suppl. **106**, 403 (2002), arXiv:hep-lat/0110115
[11] T. T. Takahashi, H. Suganuma, Y. Nemoto and H. Matsufuru, Phys. Rev. D **65**, 114509 (2002), arXiv:hep-lat/0204011[hep-lat]
[12] O. Andreev, JHEP **05**, 173 (2021), arXiv:2007.15466[hep-ph]
[13] O. Andreev, Phys. Lett. B **756**, 6 (2016), arXiv:1505.01067[hep-ph]
[14] O. Andreev, Phys. Rev. D **93**(10), 105014 (2016), arXiv:1511.03484[hep-ph]
[15] O. Andreev, Phys. Rev. D **107**(2), 026023 (2023), arXiv:2211.12305[hep-ph]
[16] O. Andreev, Phys. Rev. D **106**(6), 066002 (2022), arXiv:2205.12119[hep-ph]
[17] O. Andreev, Phys. Rev. D **108**(10), 106012 (2023), arXiv:2306.08581[hep-ph]
[18] O. Andreev, Phys. Rev. D **105**(8), 086025 (2022), arXiv:2111.14418[hep-ph]
[19] O. Andreev, Phys. Lett. B **804**, 135406 (2020), arXiv:1909.12771[hep-ph]
[20] O. Andreev, Phys. Rev. D **104**(2), 026005 (2021), arXiv:2101.03858[hep-ph]
[21] A. Yamamoto, H. Suganuma, and H. Iida, Prog. Theor. Phys. Suppl. **174**, 270 (2008), arXiv:0805.4735[hep-ph]
[22] M. Laine, PoS **LAT2006**, 014 (2006), arXiv:hep-lat/0612023
[23] T. Asaka, M. Laine, and M. Shaposhnikov, JHEP **06**, 053 (2006), arXiv:hep-ph/0605209
[24] M. Hindmarsh and O. Philipsen, Phys. Rev. D **71**, 087302 (2005), arXiv:hep-ph/0501232
[25] A. Rothkopf, Phys. Rept. **858**, 1 (2020), arXiv:1912.02253[hep-ph]
[26] T. Matsui and H. Satz, Phys. Lett. B **178**, 416 (1986)
[27] D. Kharzeev and H. Satz, *Colour Deconfinement And Quarkonium Dissociation*, arXiv: hep-ph/9505345
[28] E. Witten, Adv. Theor. Math. Phys. **2**, 505 (1998), arXiv:9803131[hep-th]
[29] F. Bigazzi, A. L. Cotrone, L. Martucci *et al.*, Fortsch. Phys. **55**, 666 (2007), arXiv:0611253[hep-th]
[30] J. M. Maldacena, Adv. Theor. Math. Phys. **2**, 231 (1998), arXiv:9711200[hep-th]
[31] O. Aharony, S. S. Gubser, J. M. Maldacena *et al.*, Phys. Rept. **323**, 183 (2000), arXiv:9905111[hep-th]
[32] J. Casalderrey-Solana, H. Liu, D. Mateos *et al.*, *Gauge/String Duality, Hot QCD and Heavy Ion Collisions*, (Cambridge University Press, 2014), ISBN 978-1-139-13674-7, arXiv: 1101.0618[hep-th]
[33] S. S. Gubser, Found. Phys. **43**, 140 (2013), arXiv:1103.3636[hep-th]
[34] H. Liu, K. Rajagopal, and U. A. Wiedemann, Phys. Rev. Lett. **98**, 182301 (2007), arXiv:0607062[hep-ph]
[35] S. I. Finazzo and J. Noronha, JHEP **01**, 051 (2015), arXiv:1406.2683[hep-th]
[36] L. Thakur, N. Haque, and H. Mishra, Phys. Rev. D **95**(3), 036014 (2017), arXiv:1611.04568[hep-ph]
[37] J. Zhou, X. Chen, Y. Q. Zhao *et al.*, Phys. Rev. D **102**(8), 086020 (2020), arXiv:2006.09062[hep-ph]
[38] S. Q. Feng, Y. Q. Zhao, and X. Chen, Phys. Rev. D **101**(2), 026023 (2020), arXiv:1910.05668[hep-ph]
[39] J. Zhou, X. Chen, Y. Q. Zhao *et al.*, Phys. Rev. D **102**(12), 126029 (2021)
[40] K. Bitaghsir Fadafan and S. K. Tabatabaei, J. Phys. G **43**(9), 095001 (2016), arXiv:1501.00439[hep-th]
[41] M. A. Escobedo, F. Giannuzzi, M. Mannarelli *et al.*, Phys. Rev. D **87**(11), 114005 (2013), arXiv:1304.4087[hep-ph]
[42] X. Chen, L. Zhang, D. Li *et al.*, JHEP **07**, 132 (2021), arXiv:2010.14478[hep-ph]
[43] X. Chen, S. Q. Feng, Y. F. Shi *et al.*, Phys. Rev. D **97**(6), 066015 (2018), arXiv:1710.00465[hep-ph]
[44] T. Song, Y. Park, S. H. Lee *et al.*, Phys. Lett. B **659**, 621 (2008), arXiv:0709.0794[hep-ph]
[45] M. Ali-Akbari, D. Giataganas, and Z. Rezaei, Phys. Rev. D **90**(8), 086001 (2014), arXiv:1406.1994[hep-th]
[46] O. Andreev, Nucl. Phys. B **977**, 115724 (2022), arXiv:2106.14716[hep-ph]
[47] C. Krishnan, JHEP **12**, 019 (2008), arXiv:0809.5143[hep-th]
[48] X. Yao and T. Mehen, JHEP **02**, 062 (2021), arXiv:2009.02408[hep-ph]
[49] M. Chernicoff, D. Fernandez, D. Mateos *et al.*, JHEP **01**, 170 (2013), arXiv:1208.2672[hep-th]
[50] S. C. Benzahra, Afr. J. Math. Phys. **1**, 191 (2004), arXiv:0204177 [hep-ph]
[51] O. Andreev, Phys. Lett. B **659**, 416 (2008), arXiv:0709.4395[hep-ph]
[52] X. Chen, B. Yu, P. C. Chu *et al.*, Chin. Phys. C **46**(7), 073102 (2022), arXiv:2112.06234[hep-ph]
[53] O. Andreev, Phys. Rev. D **76**, 087702 (2007), arXiv:0706.3120[hep-ph]
[54] E. Witten, JHEP **02**, 006 (1998), arXiv:9712028[hep-th]
[55] S. Gukov, M. Rangamani, and E. Witten, JHEP **12**, 025 (1998), arXiv:9811048[hep-th]
[56] O. Andreev, Phys. Rev. D **101**(10), 106003 (2020), arXiv:2003.09880[hep-ph]
[57] J. Erlich, E. Katz, D. T. Son *et al.*, Phys. Rev. Lett. **95**, 261602 (2005), arXiv:0501128[hep-ph]
[58] X. Cao, M. Baggioli, H. Liu *et al.*, JHEP **12**, 113 (2022), arXiv:2210.09088[hep-ph]
[59] X. Cao, J. Chao, H. Liu *et al.*, Phys. Rev. D **107**(8), 086001 (2023), arXiv:2204.11604[hep-ph]
[60] Y. Yang and P. H. Yuan, JHEP **12**, 161 (2015), arXiv:1506.05930[hep-th]
[61] O. Andreev and V. I. Zakharov, JHEP **04**, 100 (2007), arXiv:hep-ph/0611304[hep-ph]
[62] P. Colangelo, F. Giannuzzi, and S. Nicotri, Phys. Rev. D **83**, 035015 (2011), arXiv:1008.3116[hep-ph]
[63] O. Andreev and V. I. Zakharov, Phys. Lett. B **645**, 437 (2007), arXiv:0607026[hep-ph]

[64] C. Ewerz, O. Kaczmarek, and A. Samberg, JHEP **03**, 088 (2018), arXiv:1605.07181[hep-th]
[65] S. He, M. Huang, and Q. s. Yan, Prog. Theor. Phys. Suppl. **186**, 504 (2010), arXiv:1007.0088[hep-ph]
[66] D. Li, S. He, M. Huang *et al.*, JHEP **09**, 041 (2011), arXiv:1103.5389[hep-th]
[67] K. B. Fadafan, Eur. Phys. J. C **71**, 1799 (2011), arXiv:1102.2289[hep-th]
[68] K. B. Fadafan and E. Azimfard, Nucl. Phys. B **863**, 347 (2012), arXiv:1203.3942[hep-th]
[69] R. G. Cai, S. He, and D. Li, JHEP **03**, 033 (2012), arXiv:1201.0820[hep-th]